MINISTRY OF EDUCATION AND TRAINING

VIETNAM ACADEMY OF SCIENCE AND TECHNOLOGY

GRADUATE UNIVERSITY SCIENCE AND TECHNOLOGY

Nguyen Thi Xuan

STUDY THE CHARACTERISTICS OF SOME NUCLEAR REACTIONS WITH BREMSSTRAHLUNG END-POINT ENERGIES ABOVE THE GIANT DIPOLE RESONANCE AND WITH PROTON ENERGIES UP TO 45 MeV

Major: Atomic and nuclear physics

Code: 9440106

SUMMARY OF ATOMIC AND NUCLEAR PHYSICS DOCTORAL THESIS

Hanoi - 2023

The work was completed at: Graduate University of Science and Technology - Vietnam Academy of Science and Technology

Science instructor 1: Assoc.Prof. Dr. Pham Duc Khue
Science instructor 2: Prof. Dr. Nguyen Van Do

Reviewer 1:
Reviewer 2:
Reviewer 3:

The thesis will be defended before the Doctoral Thesis Assessment Committee, meeting at the Graduate University of Science and Technology - Vietnam Academy of Science and Technology on ……...…, date ……../……./2023
The thesis can be found at:
- Library of Graduate University of Science and Technology
- National Library of Vietnam

INTRODUCTION

1. Motivation

Nuclear reactions change the nuclei and emit nucleons and radiations which carry important information related the nucleus and the reaction process. The measurement and analysis of those nucleons and radiations can help to understand the characteristics of nuclear reactions and reaction mechanisms. Most of the reaction products are radioactive isotopes, which have potential applications in many different fields, including energy and non-energy sectors, as well as nuclear medicine. Currently, nuclear reactions have become the focus of nuclear science and technology research. That is why it is very necessary to conduct research on nuclear reactions in our country.

2. Objectives of the thesis

- Determination of some characteristic parameters of nuclear reactions caused by bremsstrahlung with end-point energies of 50 to 70 MeV and by protons with energies ranging from the reaction threshold to about 45 MeV. The determined parameters include reaction cross section, integrated cross section, reaction yield and yield ratio of the isomer pairs.
- Comparison of the experimental results obtained with other experimental results and theoretical predictions using the TALYS code to assess the reliability of the current experimental results, as well as the effect of the excitation energy and the reaction channel effect on the characteristic parameters of the reactions at the energies above the GDR range.
- Contribution of new, accurate nuclear data to the international nuclear library.

3. The main research contents of the thesis

In this thesis, the activation method combined with off-line gamma spectroscopy was used for the studies. The main research contents of the thesis are as follows:

1. Study on the determination of the yield of photonuclear reactions: $^{nat}Sr(\gamma,xnyp)^{82}Sr$, $^{83(m+g)}Sr$, ^{85m}Sr, ^{85g}Sr, ^{87m}Sr, $^{81(g+0.976m)}Rb$, ^{82m}Rb, ^{83g}Rb, $^{84(m+g)}Rb$ with bremsstrahlung end-point energies of 55-, 60-, and 65 MeV.
2. Study on the determination of the yield ratios for the isomeric pairs (1) $^{137m,g}Ce$ in $^{141}Pr(\gamma,X)^{137m,g}Ce$ reactions with bremsstrahlung end-point energies of 50, 60, and 70 MeV, and (2) $^{179m,g}W$ in $^{nat}W(\gamma,xn)^{179m,g}W$ reactions with bremsstrahlung end-point energies of 50, 55, 60, and 65 MeV.
3. Study on the measurement of the integrated cross section of the (1) $^{110}Pd(\gamma,n)^{109m}Pd$, $^{110}Pd(\gamma,n)^{109g}Pd$ and $^{110}Pd(\gamma,X)^{108m}Rh$ reactions with a bremsstrahlung end-point energy of 70 MeV, and (2) $^{197}Au(\gamma,xn)^{197-x}Au$ reactions with a bremsstrahlung end-point energy of 60 MeV.
4. Study on the determination of the excitation function of nuclear reactions (1) $^{nat}Pd(p,X)^{100m,g}Rh$ in the energy range from 21.09 to 42.61 MeV, and (2) $^{nat}Zr(p,X)$ ^{95}Zr, ^{95m}Nb, ^{95g}Nb in the energy range from 10.6 MeV to 43.6 MeV, and their thick target yields.

4. Structure of the thesis

The thesis is organized as follows: Chapter 1 gives an overview of the main characteristics of nuclear reactions. Chapter 2 describes the experimental methods used in the studies and the TALYS code used in the calculations. Chapter 3 presents typical results of some photonuclear reactions. Chapter 4 presents the results of the protons induced reactions. Finally, some conclusions and prospects are drawn.

CHAPTER I. OVERVIEW

1.1. Some basic characteristics of nuclear reactions

The nuclear reaction is a process of interaction between the incident particle/radiation and the target nucleus occurring at a distance within the nuclear radius (about 10^{-15}m). This process profoundly changes the nucleus involved in the reaction.

Consider a nuclear reaction: A(a,b)B (1.1)

Reaction energy (Q) is determined by:

$$Q = E_{01} - E_{02} = [(m_a + M_A) - (m_b + M_B)].c^2 = T_2 - T_1 \quad (1.2)$$

If Q > 0: the reaction is called exoergic, Q < 0: endoergic, and Q = 0: elastic scattering.

For an endoergic reaction, the incident particle needs a minimum kinetic energy (called the threshold energy E_{th}) for the reaction to take place:

$$(T_a)_{\min} = E_{th} = \frac{m_a + M_A}{M_A}|Q| \quad (1.3)$$

The reaction mechanism varies with the energy of the incident particle. The three main mechanisms used to explain nuclear reactions include the compound, direct, and pre-equilibrium.

1.2. Cross section and yield of nuclear reactions

The cross-section of reaction (σ) is the relative probability for a reaction to occur on a target nucleus per second when the flux of the incident particle/radiation is 1 particle/radiation per second [3,6] and is determined by:

$$\sigma = \frac{N_b}{\Phi.N} \quad (1.4)$$

The integrated cross section is defined as:

$$\sigma_{\text{int}} = \int_{E_{th}}^{E_{Max}} \sigma(E)\, dE \quad (1.5)$$

Reaction yield is the number of reactions occurring on the target in a unit of time. When flux and incident particle energy are constant, the yield of reaction is determined by the formula:

$$Y = \eta.N.\sigma.\Phi \quad (1.6)$$

For photonuclear reactions, the yield of reaction is calculated according to the following formula [3,6, 30-41]:

$$Y = \eta N \int_{Eth}^{Emax} \sigma(\mathrm{E})\Phi(\mathrm{E})\, dE \quad (1.7)$$

1.3. Nuclear isomers and isomeric yield ratio

The radionuclide that exits in both metastable (or isomeric) and unstable ground states is called the isomeric nuclide. The cross section for the population of the isomeric state, σ_m relative to that of the ground state, σ_g is defined as the isomeric ratio, namely:

$$IR = \sigma_m / \sigma_g \quad (1.8)$$

In the case of a bremsstrahlung-induced reaction, the isomeric yield ratio is used, i.e. [3,6]:

$$IR = Y_{highspin} / Y_{low\,spin} \quad (1.9)$$

CHAPTER 2. METHODS FOR THE STUDY

In the study, experimental measurements were carried out in combination with model calculations. Measurements are made using the activation method. Calculations are performed using the TALYS code.

2.1. Experimental study using activation method

2.1.1. Activation method

Based on the fact that most of the reaction products are radioactive isotopes. By measuring and analyzing the gamma spectra of the radioactive products, we can identify the nuclides produced and determine their activities. Thus, it is also possible to determine the characteristic parameters of nuclear reactions.

The relation between the photo-peak area of the gamma ray and the radioactivity of reaction product can be related as [1]:

$$C = \frac{N_0 \Phi \sigma \varepsilon I_\gamma f \left(1 - e^{-\lambda t_i}\right) e^{-\lambda t_w} \left(1 - e^{-\lambda t_m}\right)}{\lambda} \quad (2.1)$$

If the incoming projectile follows the pulsed mode with the width of the pulse τ, the cycle period T, and the irradiation, waiting, and counting time of t_i, t_w, and t_m, and f is the correction factor for counting losses, the photo-peak area is determined as:

$$C_{pulse} = \frac{N_0 \Phi \sigma \varepsilon I_\gamma f \left(1 - e^{-\lambda \tau}\right) e^{-\lambda (T-\tau)} \left(1 - e^{-\lambda t_i}\right) e^{-\lambda t_w} \left(1 - e^{-\lambda t_m}\right)}{\lambda \left(1 - e^{-\lambda T}\right)} \quad (2.2)$$

2.1.2. The irradiation with bremsstrahlung photon

The 100 MeV electron linac-based bremsstrahlung source at the Pohang Accelerator Laboratory (PAL), Korea was used for the irradiation. The bremsstrahlung was generated by bombarding an electron beam on the W target which is 100 mm × 100 mm in size and 0.1 mm thick. High purity (≥ 99.9%) natural samples of ^{nat}Sr, ^{nat}Pr, ^{nat}W, ^{nat}Pd and ^{nat}Au with a size of ≤ 15 mm × 15 mm and a thickness of ≤ 0.1 mm were irradiated with the bremsstrahlung end-point energies in the range of 50-70 MeV. The irradiation arrangement is shown in Fig. 2.5.

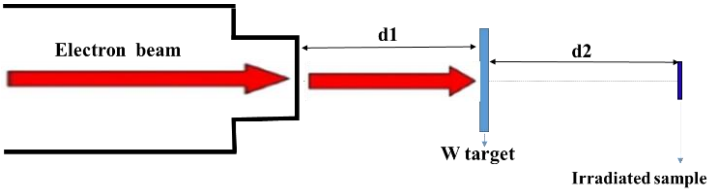

Fig. 2.5. The experimental arrangement for the irradiation on the linac 100 MeV electron linac

In general, the W target was placed 15 cm from the electron beam exit window during irradiation, and the sample was placed 12 cm from the W target. Depending on the application, the

electron beam current can be selected in the range of 25 - 35 mA, the beam pulse width of 1.2 μs and a repetition rate of 30 Hz.

2.1.3. The irradiation with proton beam

Irradiation with a proton beam was carried out at the MC-50 cyclotron of the Korea Institute of Radiological and Medical Sciences, Korea (KIRAMS). A sample stack containing the following W–Zr–Y–Pd–Cu–Al foils was irradiated with a 45 MeV proton beam. Besides Pd and Zr samples, Cu and Al were used as monitors. Additionally, all metallic foils, including samples, are responsible as energy degraders. All foils used were supplied by the manufacturer Alfa Aesar with the same size of 10 mm × 10 mm. The setup for irradiating stacked foils is shown in Fig. 2.7 [102].

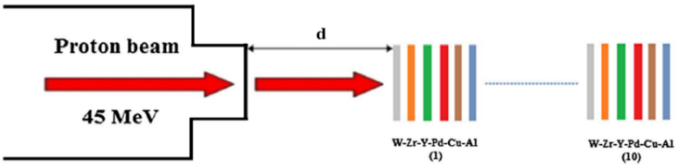

Fig. 2.7. The experimental arrangement for the irradiation of stacked-foils with proton beams on MC-50

Proton energies along the foil stack were calculated using the computer code SRIM-2003 [99]. The energies of the proton beam entering the first and last Zr in the stack were calculated as 43.6 ± 0.4; 10.6 ± 1.3 MeV, and for the Pd are 42.61 ± 0.49; 8.37 ± 1.57 MeV, respectively. The proton beam flux entering each foil was determined via the monitoring reactions $^{nat}Cu(p,X)^{62}Zn$ and $^{nat}Cu(p,X)^{65}Zn$.

2.1.4. Measurement and analysis of the gamma spectrum

The gamma rays of reaction products from the irradiated samples were measured by the energy and efficiency calibrated HPGe detector (model ORTEC, GEM-20180-p) coupled with a

PC 4K channel analyzer. The energy resolution of the detector system was 1.8 keV at 1332.5 keV of ^{60}Co, and the detection efficiency was 20% at 1332.5 keV relative to that of a 7.6 cm × 7.6 cm NaI(Tl) detector. The total and photo-peak efficiencies of the HPGe detector were calibrated using the following set of standard gamma sources: ^{241}Am (59.541 keV), ^{137}Cs (661.657 keV), ^{60}Co (1,173.237 keV and 1,332.501 keV), ^{152}Eu (121.8–1,408 keV), and ^{133}Ba (53.16 – 388.85 keV). The measured gamma spectra were analyzed using softwares GammaVision version, Fitzpeaks and Origin. Radioisotopes formed in reactions were identified based on their half-lives and gamma-radiation energies. The reaction cross-section and/or the reaction yield are determined from the measured activity of the reaction products.

2.1.5. Some corrections for radioactive activity measurements

In order to improve the accuracy of the measurement results, necessary corrections were made, such as the dead time of the detection system, the self-absorption of gamma rays, the coincidence summation effect, the variation of beam flux, gamma ray interference and the contribution of decay activity.

2.5. Comparison of experimental results with theoretical predictions using the TALYS code

The cross-sections of the studied reactions were calculated using the TALYS code [46-48]. The input parameters were taken from the standard RIPL-3 library [45]. The effects of level density models and gamma ray strength functions were taken into account for most of the calculations. In addition, the bremsstrahlung spectrum required for some studies was simulated by the MCNPX code [49], and the proton beam energy at each foil in the sample stack was calculated using the SRIM-2003 code [99].

CHAPTER 3. RESEARCH RESULTS OF SOME PHOTONUCLEAR REACTIONS

This chapter summarizes the research results on determining the characteristics of photonuclear reactions with bremsstrahlung end-point energies in the range of 50-70 MeV.

3.1. Yields of ^{nat}Sr(γ, xnyp) reactions.

The thesis has determined the yields of the reaction products ^{82}Sr, $^{83(m+g)}$Sr, ^{85m}Sr, ^{85g}Sr, ^{87m}Sr, $^{81(g+0.976m)}$Rb, ^{82m}Rb, ^{83g}Rb, $^{84(m+g)}$Rb and $^{86(m+g)}$Rb in ^{nat}Sr(γ,xnyp) reactions with bremsstrahlung end-point energies of 55, 60, and 65 MeV. The current results are the first measurement [51].

Table 3.2. Yields of the ^{nat}Sr(γ,xnyp) reactions.

Reaction products	Yields (kBq.μA^{-1}.h^{-1}.mg^{-1})		
	55 MeV	60 MeV	65 MeV
^{87m}Sr	16.09 ± 1.93	16.39 ± 1.97	17.03 ± 2.04
^{85m}Sr	1.92 ± 0.25	2.04 ± 0.27	2.05 ± 0.27
^{85g}Sr	1.29 ± 0.19	1.44 ± 0.22	1.49 ± 0.22
$^{83(m+g)}$Sr	0.18 ± 0.02	0.202 ± 0.022	0.22 ± 0.02
^{82}Sr	0.023 ± 0.004	0.027 ± 0.005	0.029 ± 0.005
$^{86(m+g)}$Rb	0.17 ± 0.03	0.21 ± 0.03	0.23 ± 0.04
$^{84(m+g)}$Rb	0.048 ± 0.007	0.082 ± 0.012	0.102 ± 0.018
^{83g}Rb	(40 ± 5).10^{-3}	(52 ± 6).10^{-3}	(71 ± 8).10^{-3}
^{82m}Rb	(243 ± 35).10^{-5}	(44 ± 6).10^{-4}	(68 ± 9).10^{-4}
$^{81(g+0.976m)}$Rb	(241 ± 35).10^{-5}	(38 ± 6). 10^{-4}	(59 ± 9).10^{-4}

Production yields of ^{nat}Sr(γ,xnyp) reactions were also calculated using the TALYS-1.95 code in combination with six different level-density models. The calculated results are plotted

in Fig. 3.5 and Fig. 3.6 along with experimental results for comparison.

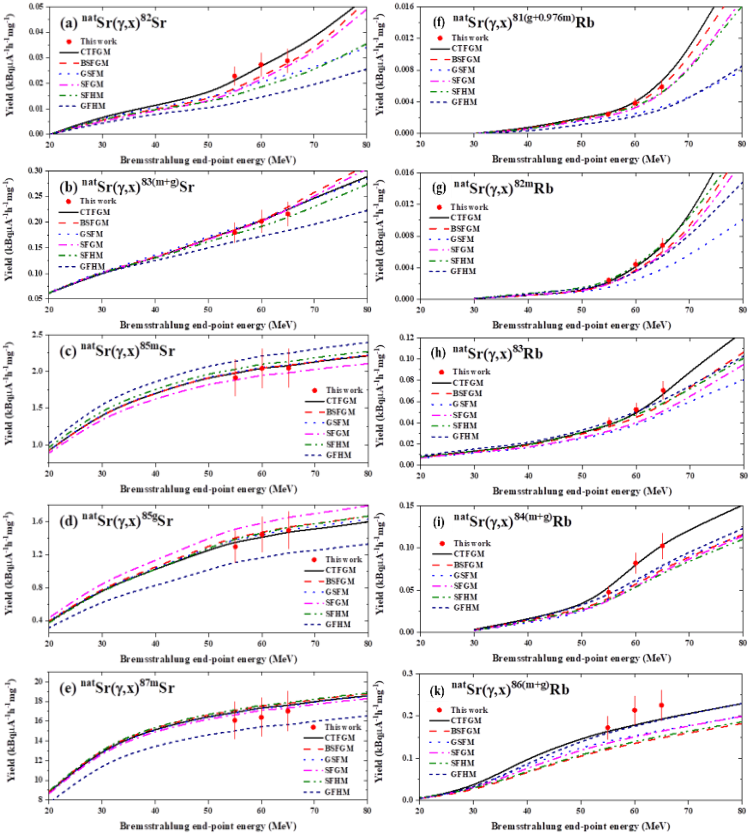

Fig. 3.5. and ***3.6.*** Measured and calculated yield values for the (a) ^{82}Sr, (b) $^{83(m+g)}$Sr, (c) ^{85m}Sr, (d) ^{85g}Sr, (e) ^{87m}Sr, (f) $^{81(g+0.976m)}$Rb, (g) ^{82m}Rb, (h) ^{83}Rb, (i) $^{84(m+g)}$Rb, and (k) $^{86(m+g)}$Rb in ^{nat}Sr(γ,xnyp) reactions. The calculations were performed using the TALYS-1.95 code in conjunction with six different level-density models [51].

It is found that, the agreement between the measured and calculated yields for all the radioisotopes was acceptable, except

for the results calculated with the GFHM level-density model. The calculated results performed with the CTFGM level density model are in good agreement with most of the measured results. Within the studied energy range, the measured and calculated yield values showed an increasing trend. The reason can be attributed to the opening of new reaction channels with increasing threshold energy. Moreover, the yield of multi-particle reactions decreased as the number of nucleons released from the target nucleus increased.

It was found that some radioisotopes such as ^{87m}Sr, ^{85m}Sr, ^{83}Sr, ^{82}Sr/^{82}Rb, and ^{81}Rb, are promising medical isotopes. Thus, in addition to providing new data, the present study also provides an additional method for the production of useful medical isotopes from natural strontium via photonuclear reactions.

3.2. Yield ratio of the isomeric pairs.

3.2.1. Yield ratio of the isomeric pair ^{137m,g}Ce.

We measured the isomeric yield ratio of the ^{137m,g}Ce isomeric pair formed in the ^{141}Pr(γ,X) reaction with bremsstrahlung end point energies of 50-, 60-, and 70 MeV. The experiment focused on the accurate activity measurement of the ^{137m}Ce and ^{137g}Ce states, using the corresponding gamma rays of 254.29 keV (11.1%) and 447.15 keV (1.68%), respectively. For this purpose, corrections for overlapping gamma rays were made [52].

For comparison, theoretical predictions were made. For the calculation, the cross section for the formation of the two states was calculated using the statistical model code TALYS combined with six level density models (LDMD1-6). The bremsstrahlung spectra emitted by the W target bombarded by 50, 60 and 70 MeV electron beams were simulated using the MCNPX code. The experimental results obtained by the two

different activity correction methods, called (1) peak-to-peak ratio relationship (PTPRR), and (2) different half-life relationship (DHLR) and by TALYS calculation using the CTFGM level density model are given in Table 3.4.

Table 3.4. Yield ratio of the isomeric pair ^{137m,g}Ce produced in the ^{141}Pr(γ,X)^{137m,g}Ce [52].

Isomeric pair ^{137m,g}Ce produced in ^{141}Pr(γ,p3n) reaction	$E_{\gamma max}$ (MeV)	Isomeric yield ratio		
		(PTPRR)	(DHLR)	TALYS (CTFGM)
	50	0.95±0.14	0.96±0.15	1.07
	60	1.42±0.18	1.39±0.17	1.61
	70	1.78±0.22	1.79±0.20	1.90

For better visualization, the measured and calculated results are plotted in Fig. 3.11.

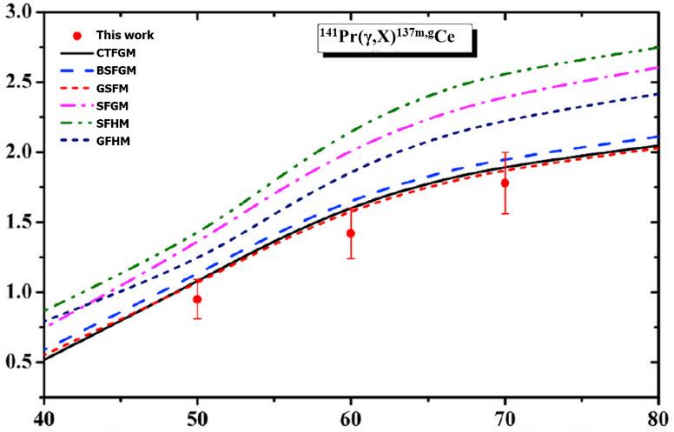

Fig. 3.11. Measured and calculated isomeric yield ratio of the ^{137m,g}Ce isomeric pair in the ^{141}Pr(γ,X) reaction.

3.2.2. Yield ratio of the isomeric pair ^{179m,g}W.

The isomeric yield ratios for the isomeric pair ^{179m,g}W produced in the ^{nat}W(γ,xn)^{179m,g}W reactions were measured with 50, 55, 60, and 65 MeV bremsstrahlung end-point energies. The activities of the ^{179m}W and ^{179g}W states were measured from the corresponding gamma rays of 221.5 keV (8.8%) and 133.9 keV (0.106%), respectively. To obtain the accurate measured activity, necessary corrections such as overlapping and/or interference gamma rays were made. The yield ratio of the high-spin state, ^{179g}W($J^{\pi}=7/2^{-}$) relative to that of the low-spin state, ^{179m}W(($J^{\pi}= 1/2^{-}$) are given in Table 3.6 together with previous measured data for comparison [53].

Table 3.6. Isomeric yield ratios for the ^{179m,g}W isomeric pair

Nuclear reaction	$E_{\gamma max}$ (MeV)	$IR = Y_{high\text{-}spin}/Y_{low\text{-}spin}$	
		This work	Reference
^{180}W(n,2n)^{179m,g}W	13.5 14.1		2.498 [54,55] 2.400 [54,55]
^{180}W(γ,n)^{179m,g}W	20		1.45 [56]
^{180}W(γ,n)^{179m,g}W	30		1.72 [56] 1.93 ± 0.02 [57]
^{180}W(γ,n)^{179m,g}W	40		1.82 [56]
^{nat}W(γ,xn)^{179m,g}W	50	1.90 ± 0.21	
^{nat}W(γ,xn)^{179m,g}W	55	1.89 ± 0.20	
^{nat}W(γ,xn)^{179m,g}W	60	1.96 ± 0.19	
^{nat}W(γ,xn)^{179m,g}W	65	2.03 ± 0.19	

As seen in Table 3.6, there is no data measured with energies higher than 40 MeV bremsstrahlung end-point energies. The present results are the first measurement in the energy range 50-65 MeV. Current results help to extend our understanding of how the isomeric yield ratios depend on the incident bremsstrahlung end-point energies in the energy region just above the GDR.

3.3. Integrated cross section of the photonuclear reactions

3.3.1. Integrated cross section of the $^{110}Pd(\gamma,n)^{109m,g}Pd$, and $^{110}Pd(\gamma,X)^{108m}Rh$ reactions.

The integrated cross sections of the $^{110}Pd(\gamma,n)^{109m}Pd$, $^{110}Pd(\gamma,n)^{109g}Pd$ and $^{110}Pd(\gamma,X)^{108m}Rh$ reactions in the energy range from the reaction threshold to 70 MeV bremsstrahlung end-point energy have been measured relative to that of the monitor reaction $^{27}Al(\gamma,X)^{24}Na$. The activities of the ^{109m}Pd, ^{109g}Pd, and ^{108m}Rh were measured using corresponding gamma-rays of 188.9 keV, 88.03 keV, and 581.1 keV, respectively.

Table 3.8. Integrated cross sections of the $^{110}Pd(\gamma,n)^{109m}Pd$, $^{110}Pd(\gamma,n)^{109g}Pd$ and $^{110}Pd(\gamma,X)^{108m}Rh$ reactions [58].

Nuclear reaction	$E_{\gamma max}$ (MeV)	Integrated cross section (mb.MeV)	
		Current result	Reference
$^{110}Pd(\gamma,n)^{109m}Pd$	70	110.80±12.99	-
	28.75	-	137.64 [62]
	25	-	77±8 [63]
	18	-	69.36 [64]
$^{110}Pd(\gamma,n)^{109g}Pd$	70	970.21±96.47	-
	25	-	1100±100 [65]
$^{110}Pd(\gamma,X)^{108m}Rh$	70	6.70 ± 0.79	-

For comparison purpose, theoretical calculations were also made using the statistical nuclear model code TALYS-1.9. During the calculation, six different level density models combined with eight gamma strength functions were calculated and a dataset of 48 calculated results for each reaction was obtained. The comparison shows that the results calculated from

the combination of the SFH level density model and the HFBCS gamma power function fit well with the current experimental results. The current results are measured for the first time with 70 MeV bremsstrahlung end-point energy. The measured and calculated results are shown in Fig 3.19 [58].

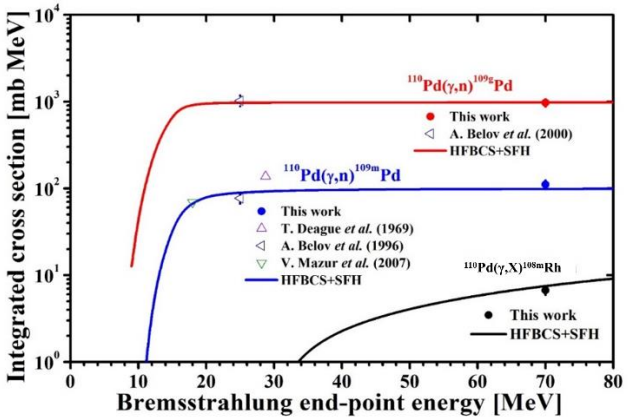

Fig. 3.19. Measured and calculated integrated cross section of the ^{110}Pd(γ,n)^{109m,g}Pd and ^{110}Pd(γ,X)^{108m}Rh reactions.

It can be seen that the integrated cross section curve for the ^{110}Pd(γ,X)^{108m}Rh reaction shows a continuous increasing trend beyond the endpoint energy of 70 MeV. However, the integrated cross section curves for the ^{110}Pd(γ,n)^{109m}Pd and ^{110}Pd(γ,n)^{109g}Pd reactions increase with increasing energy from the reaction threshold to about 20 MeV, and then appears to be unchanged. The saturation trend seems to confirm that no second peak appears after the first resonant peak in the GDR energy region. This fact also suggests that to reach the maximum activity of the medical isotope ^{109g}Pd, it is enough to use bremsstrahlung photons with an endpoint energy of about 20 MeV.

3.3.2. Integrated cross sections of $^{197}Au(\gamma,xn)^{197-x}Au$ reactions

The integrated cross sections for the production of ^{196}Au, ^{195}Au, ^{194}Au, ^{193}Au, ^{192}Au, ^{191}Au, and ^{190}Au from the ^{197}Au(γ,xn) reactions were measured using the activation method in combination with off-line gamma-ray spectrometric technique. The experiment was performed with 60 MeV bremsstrahlung end-point energy and the integrated cross sections were determined relative to that of the ^{197}Au(γ,xn)^{196}Au reaction [70].

Table 3.9. Integrated cross sections for the ^{197}Au(γ,xn)$^{197-x}$Au reactions induced by 60 MeV bremsstrahlung end-point energy.

Nuclear reaction	Integrated cross section (mb.MeV)		Literature data measured with $E_{\gamma max}$ = 67.7MeV
	Measured	Calculated	
^{197}Au(γ, n)^{196}Au	2399.98± 264.50	2375.74	2280±200 [75] 2213±210 [74]
^{197}Au(γ,2n)^{195}Au	952.65± 123.84	944.88	730±180 [75] 567±100 [74] 902.39±108.28 (**)
^{197}Au(γ,3n)^{194}Au	232.85± 25.61	226.89	240±30 [75] 181± 30 [74]
^{197}Au(γ,4n)^{193}Au	144.23± 20.82	169.81	160± 20 [75] 162± 20 [74]
^{197}Au(γ,5n)^{192}Au	100.16± 13.01	96.18	123±10 [75] 123±10 [74]
^{197}Au(γ,6n)^{191}Au	54.91± 6.21	62.08	63±15 [75] 67±15 [74]
^{197}Au(γ,7n)^{190}Au	5.41± 0.85	4.63	-

Since gold is the mono-isotopic element, it can be used as a monitoring reaction in many cases. Study of multiparticle $^{197}Au(\gamma,xn)^{197-x}Au$ reactions therefore provides information on channel effects. In addition, the nuclear data that can be used for both research and applications, including activation experiments. In addition to the measurement, the model calculation was also performed using the code TALYS-1.9. The calculations were tested with six level density models. The comparison shows that the experimental results are best suited for predictions using the TALYS code with the CTFGM level density model. In Table 3.10 we have summarized the currently measured integrated cross section, the results calculated using the TALYS code with the CTFGM level density model and the data available in the literature for comparison.

CHAPTER 4. RESEARCH RESULTS FOR NUCLEAR REACTIONS INDUCED BY PROTONS

This chapter summarizes the research results on determining the characteristics of proton-induced reactions in the energy range from the threshold to about 45 MeV.

4.1. Excitation functions of the $^{nat}Zr(p,X)^{95}Zr$, ^{95m}Nb, ^{95g}Nb reactions

We measured the independent cross sections of the $^{nat}Zr(p,X)^{95m}Nb$ and $^{nat}Zr(p,X)^{95g}Nb$ reactions as well as cumulative cross section of the $^{nat}Zr(p,X)^{95}Zr$ [89] reaction in the energy range of 10.6 to 43.6 MeV. To support the cross section measurement, the proton flux was determined by the monitoring reactions $^{nat}Cu(p,X)^{62}Zn$ and $^{nat}Cu(p,X)^{65}Zn$. The degradation of the proton energy in the foil stack was calculated using the computer code SRIM-2003. The measured cross sections are given in Table 4.2.

Table 4.2. Measured cross sections of the ^{95}Zr, ^{95m}Nb and ^{95g}Nb radionuclides formed in the ^{nat}Zr(p,X) reactions [89].

Proton energy (MeV)	Energy-dependent cross section (mb)		
	^{95}Zr	^{95m}Nb	^{95g}Nb
43.6 ± 0.4	4.83 ± 0.70	-	1.63 ± 0.23
40.7 ± 0.4	4.96 ± 0.72	-	2.05 ± 0.28
37.6 ± 0.4	4.99 ± 0.72	-	2.19 ± 0.32
34.3 ± 0.5	5.50 ± 0.76	-	2.45 ± 0.34
30.8 ± 0.5	5.31 ± 0.76	-	3.06 ± 0.40
26.9 ± 0.6	4.54 ± 0.68	0.65 ± 0.06	4.41 ± 0.63
22.5 ± 0.7	3.19 ± 0.44	1.06 ± 0.12	7.97 ± 1.10
17.3 ± 0.9	1.24 ± 0.18	3.75 ± 0.38	22.39 ± 3.15
10.6 ± 1.3	0.15 ± 0.02	5.04 ± 0.52	14.48 ± 2.05

Beside measurement, the cross sections for the ^{nat}Zr(p,X)^{95}Zr, ^{nat}Zr(p,X)^{95m}Nb and ^{nat}Zr(p,X)^{95g}Nb reactions were also calculated using the TALYS-1.9 code. In the calculations, a six-level density model was tested and found that the results obtained using the CTFGM level density model is best suited for most experimental results. The measured cross sections together with the available reference data as well as with the partial and total cross sections calculated using the TALYS-1.9 code and the TENDL-2019 data library are shown in Figs. 4.3, 4.4, and 4.5. The data presented in this thesis, are useful in nuclear model testing and in the production of radioisotopes [89].

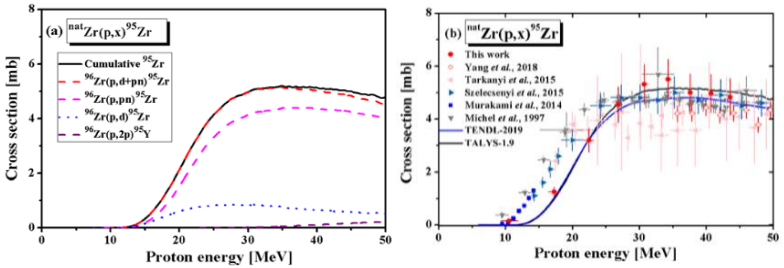

Fig. 4.3. (a) Caculated and (b) measured cross sections for the production of ^{95}Zr in the ^{nat}Zr*(p,X)* reactions

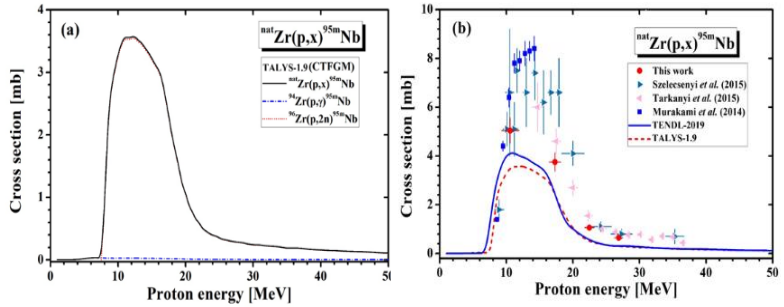

Fig 4.4. (a) Caculated and (b) measured cross sections for the production of ^{95m}Nb in the ^{nat}Zr*(p,X)* ^{95m}Nb reactions.

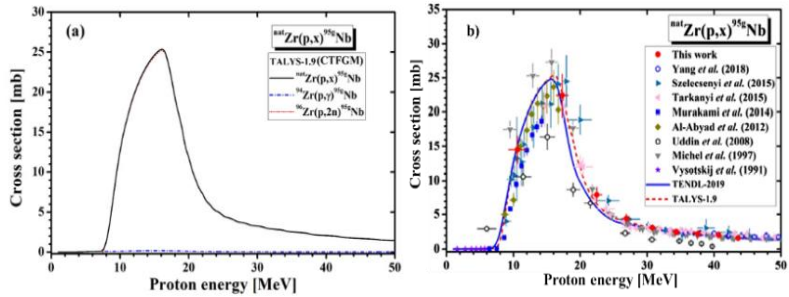

Fig 4.5. (a) Caculated and (b) measured cross sections for the production of ^{95g}Nb in the ^{nat}Zr*(p,X)* ^{95g}Nb reactions.

4.2. Thick target yields of the ^{95}Zr, ^{95m}Nb and ^{95g}Nb isotopes.

The thick target yield is defined as the activity of the reaction product at the end of irradiation, with an irradiation time of one hour and a beam current of 1 μA assuming that all energy of the incoming projectile is absorbed into that target. The measured and calculated yields for ^{95}Zr, ^{95m}Nb and ^{95g}Nb formed in the ^{nat}Zr(p,X) reactions are shown in Table 4.3 and in Fig. 4.6.

Table 4.3. Thick target yields of the ^{95}Zr, ^{95m}Nb and ^{95g}Nb isotopes produced from the ^{nat}Zr(p,X) reactions [89].

Proton energy (MeV)	Thick target yield (MBq. $\mu A^{-1} \cdot h^{-1}$)		
	^{95}Zr	^{95m}Nb	^{95g}Nb
43.6 ± 0.4	0.23 ± 0.04	-	0.65 ± 0.10
40.7 ± 0.4	0.20 ± 0.03	-	0.63 ± 0.10
37.6 ± 0.4	0.16 ± 0.03	-	0.61 ± 0.09
34.3 ± 0.5	0.13 ± 0.02	-	0.58 ± 0.09
30.8 ± 0.5	0.09 ± 0.02	-	0.55 ± 0.08
26.9 ± 0.6	0.06 ± 0.01	0.87 ± 0.15	0.51 ± 0.07
22.5 ± 0.7	0.03 ± 0.01	0.77 ± 0.12	0.43 ± 0.06
17.3 ± 0.9	0.006 ± 0.001	0.61 ± 0.07	0.26 ± 0.04
10.6 ± 1.3	$(1 \pm 0.3).10^{-4}$	0.12 ± 0.03	0.03 ± 0.01

As can be seen in Fig 4.6, the thick target yields obtained for ^{95}Zr and ^{95g}Nb isotopes agree well with theoretical calculations, while the results for ^{95m}Nb are higher than theoretical predictions.

4.3. Excitation functions of the ^{nat}Pd(γ,X)^{100g}Rh reactions.

We measured the excitation functions for the production of the ground state ^{100g}Rh from the ^{nat}Pd(p,X)^{100m,g}Rh reaction in the energy range from 21.09 to 42.61 MeV [102]. The activity of the ^{100g}Rh was measured using the γ-ray of 539.51 keV (80.6%). We

cannot separate the activity contributed from the decay of ^{100m}Rh ($T_{1/2}$=4.6 min) with an isomeric transition factor of 98.3% to the ground state ^{100g}Rh. Thus, the measurement based on the gamma ray of 539.51 keV gives a total activity of ^{100g}Rh and 98.3% of ^{100m}Rh, denoted as activity of $^{100(g+0.983m)}$Rh.

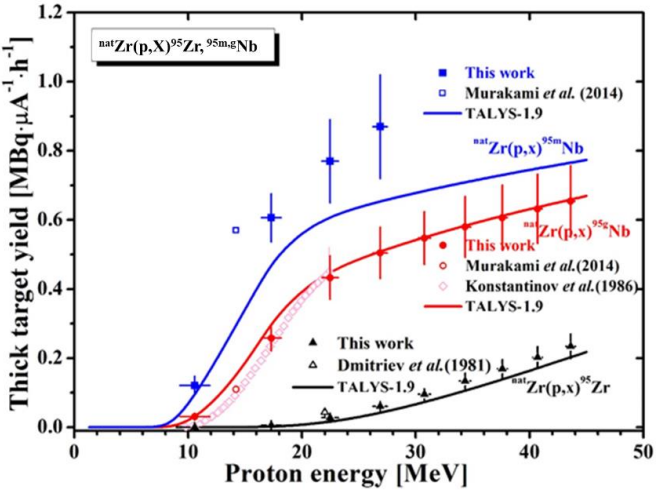

Fig 4.6. Thick target yields of the ^{95}Zr, ^{95m}Nb and ^{95g}Nb isotopes produced from the ^{nat}Zr(p,X) reactions [89].

A detailed study indicates that ^{100m,g}Ag and ^{100}Pd are also produced in the ^{nat}Pd(p,X) reactions. Both the ^{100m}Ag and ^{100g}Ag decay to ^{100}Pd and ^{100}Pd again decays to ^{100g}Rh. The total activity of ^{100m}Ag, ^{100g}Ag, and ^{100}Pd can be determined from the 84.0 keV (52%) gamma ray of the ^{100}Pd isotope. Therefore, by subtracting the activity measured from the 84.0 keV gamma ray we can obtain the activity of $^{100(g+0.983m)}$Rh.

Table 4.5. Cross-sections for the formation of the ^{100g}Rh and ^{100}Pd in the ^{nat}Pd(p,X) reactions [102].

Proton energy (MeV) [1]	$\sigma_{sum}(^{(100g+0.983m)}Rh)$ cross section (mb)		$\sigma_{cum}(^{100}Pd)$ cross section (mb)	
	Experi-mental [2]	TENDL-2017 [3]	Experi-men-tal [4]	TENDL2017[5]
15.72±1.00	-	-	-	-
21.09±0.81	1.85 ± 0.46	1.95	-	0.004
25.61±0.69	5.11±0.68	4.24	0.44 ± 0.11	1.23
29.60±0.65	9.59±1.51	8.08	1.92 ± 0.38	4.77
33.23±0.57	10.56±2.16	11.23	4.09 ± 0.61	6.28
36.54±0.54	11.25±2.53	12.31	5.22 ± 0.73	5.94
39.70±0.51	13.71±2.62	12.87	4.66 ± 0.65	5.03
42.61±0.49	14.54±2.53	13.64	3.96±10.55	4.31

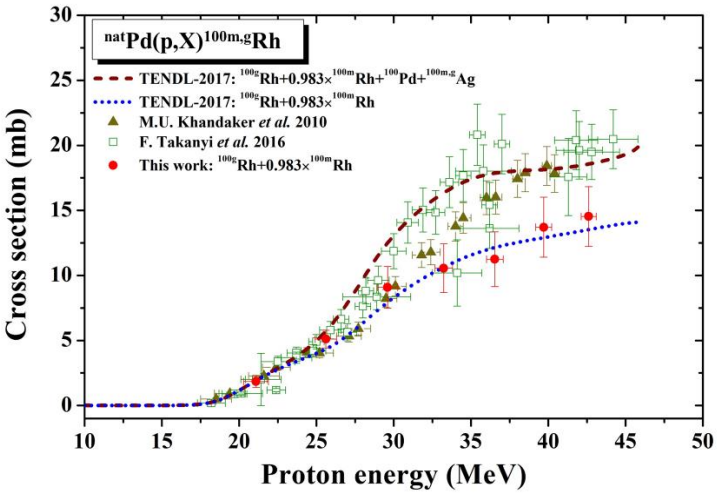

Fig. 4.8. Excitation function of the $^{nat}Pd(\gamma,X)^{100m,g}Rh$ reactions in the energy range from 10 to about 45 MeV.

From the measured activities mentioned above, we can determine the total cross sections for the formation of $^{100(g+0.983m)}$Rh, denoted $\sigma_{sum}(^{(100(g+0.983m)}Rh)$, and the cumulative cross section for the formation of ^{100}Pd, denoted $\sigma_{cum}(^{100}Pd)$. The obtained results are given in Table 4.5. The excitation function for the formation of (^{100g}Rh+0.983x^{100m}Rh) and that for all reaction channels leading to the formation of ^{100g}Rh are shown in Fig. 4.8.

CONCLUSIONS AND OUTLOOK

The thesis presented the research results of some nuclear reactions with bremsstrahlung end-point energies above the giant dipole resonance and with proton energies up to 45 MeV. The main results of the thesis can be summarized as follows:

1.1. Yields of 10 reaction products in the ^{nat}Sr(g,xnyp) reactions were measured with maximum bremsstrahlung energies of 55, 60 and 65 MeV [51]. They are measured for the first time.

1.2. Yield ratio of the isomeric pair ^{137m,g}Ce produced in the reaction ^{141}Pr(γ,X) were measured with bremsstrahlung end-point energies of 50, 60 and 70-MeV [52] and ^{179m,g}W produced in the ^{nat}W(γ,xn) with bremsstrahlung end-point energies of 50, 55, 60 and 65-MeV [53]. They are measured for the first time.

1.3. The integrated cross section of ^{110}Pd(γ,n)^{109m,g}Pd and ^{110}Pd(γ,X)^{108m}Rh reactions with 70 MeV bremsstrahlung end-point energy [58] and ^{197}Au(γ,xn)$^{197-x}$Au reactions 60 MeV bremsstrahlung end-point energy were measured [70].

1.4. Excitation functions were measured for (1) the nuclear reactions ^{nat}Zr(p,X)^{95}Zr,^{95m}Nb, ^{95g}Nb in the energy range

10.6 MeV to 43.6 MeV [89] and (2) the nuclear reaction ^{nat}Pd(p,X)^{100m,g}Rh in the energy range 21,09 to 42.61 MeV [102].

1.5. Thick target yields for ^{nat}Zr(p,X)^{95}Zr,^{95m}Nb,^{95g}Nb reactions in the energy range 10.6 MeV to 43.6 MeV were also measured and calculated using the TALYS code [89].

The results obtained are compared to calculations using the TALYS code, taking into account six level density models and eight gamma strength functions. The thesis has collected more than 100 nuclear data published in 07 scientific articles. Most current data is the first measurement. They have relatively high accuracy and hope to be used in scientific research and various application areas, including nuclear model validation and medical radioisotope production.

Based on the analysis of photonuclear data, it helps to understand the role of excitation energy for the reaction mechanism. In the energy range beyond the giant resonance region, the role of direct and pre-equilibrium mechanisms increases in addition to the compound.

As can be seen, in the energy range above the giant dipole resonance range, the reaction mechanisms are more complicated, but the nuclear data required for the analysis are not sufficient, so new data must be provided. The author intends to continue the study of nuclear reactions using medium and high energy particles/radiation, combined with theoretical calculations to further investigate nuclear reactions, and provide new data for research and for applications.

SCIENTIFIC WORKS RELATED TO THE THESIS

1. N.V. Do, N.T. Luan, N.T. Xuan, K.T. Thanh, N.T. Hien, G. Kim. *Multiparticle $^{nat}Sr(\gamma,xnyp)$ reactions induced with bremsstrahlung end-point energies of 55, 60, and 65 MeV*. Chinese Physics C, 2022, 46(9), 094003.
2. N.V. Do, N.T. Luan, N.T. Xuan, P.D. Khue, N.T. Hien, G. Kim, M.H. Cho. *Measurement of yield ratios for the isomeric pair $^{137m,g}Ce$ in the $^{141}Pr(\gamma,X)^{137m,g}Ce$ reaction induced with 50-, 60-, and 70 MeV bremsstrahlung end-point energies.* Radiat. Phys. Chem, 2020, 176, 109016
3. N.V. Do, P.D. Khue, N.T. Xuan, B.V. Loat, N.T. Hien, G. Kim. *Yield ratios of the isomeric pair $^{179m,g}W$ produced in the $^{nat}W(\gamma,xn)^{179m,g}W$ reactions with 50-65 MeV Bremsstrahlung.* Commun. Phys, 2017, 27(3), 181-191.
4. N.V. Do, N.T. Luan, N.T. Xuan, K.T. Thanh, B.V. Loat, N.T. Hien, G. Kim. *Measurement of the integrated cross section of $^{110}Pd(\gamma,n)^{109m}Pd$, $^{110}Pd(\gamma,n)^{109g}Pd$, and $^{110}Pd(\gamma,X)^{108m}Rh$ reactions with 70 MeV bremsstrahlung*. Radiat. Phys. Chem, 2023, 203A, 110598.
5. N.V. Do, N.T. Luan, N.T. Xuan, P.D. Khue, K.T. Thanh, B.V. Loat, N.T. Hien, G. Kim. *Integrated cross sections of the photo-neutron reactions induced on ^{197}Au with 60 MeV bremsstrahlung.* Communi. Phys, 2020, 30, 49-60.
6. N.V. Do, N.T. Luan, N.T. Hien, G. Kim, N.T. Xuan, K.T. Thanh. *Excitation functions and thick target yields of the $^{nat}Zr(p,X)$ ^{95}Zr, ^{95m}Nb, ^{95g}Nb reactions.* Eur. Phys. J. A, 2020, 56, 194.
7. N.V. Do, N.T. Luan, N.T. Xuan, N.T. Hien, G. Kim, K. Kim. *Measurement of cross sections for the formation of ^{100g}Rh in $^{nat}Pd(p,X)^{100m,g}Rh$ reactions up to 42,61 MeV.* J. Radioanal. Nucl. Chem, 2019, 321, 117-123.